



A Study of Ultrafast Ablation on ITO Thin Films with Wavelengths of 513 and 1026 nm for High Resolution Patterning

Junha Choi^{1,2} · Sung-Hak Cho^{1,2}

Received: 16 May 2023 / Revised: 28 July 2023 / Accepted: 28 July 2023 / Published online: 14 August 2023
© The Author(s), under exclusive licence to Korean Society for Precision Engineering 2023

Abstract

Indium tin oxide (ITO) exhibits transparency and high electrical conductivity in the visible and near-IR wavelength ranges. Therefore, ITO is used in liquid crystal displays, organic light-emitting diodes, photovoltaics, and solar cells. However, ITO must be partially ablated before employing it in applications. High-resolution patterning technology is required to obtain the desired ITO morphology, and accordingly, various technologies have been developed. Recently, ultrafast lasers have been widely used for controlled ablation because of their non-thermal properties caused by short pulse widths. This study analyzes the changes in ablation characteristics as a function of various parameters such as pulse energy, pulse duration, number of pulses, and wavelength. We show that the optimized ablation characteristics could lead to the efficient formation of the desired morphology of ITO.

Keywords Laser ablation · Pulse energy · Pulse duration · Number of pulses · Non-thermal property

1 Introduction

Indium tin oxide (ITO) is widely used in liquid crystal displays (LCDs), organic light-emitting diodes (OLEDs), photovoltaics, and solar cells because of its transparency and high electrical conductivity in the visible and near-IR wavelength ranges [1–6]. Prior to use in applications, ITO should be conducted partial ablation, and high-resolution patterning technology is required to obtain the desired ablation size and edge of ITO and to improve transparency and electrical conductivity [7, 8]. For instance, conventional photolithography with wet etching for microstructure processing is declining due to its complexity, high cost, and the chemicals used in the process [9]. Pulse laser ablation is a

simple, fast, non-chemical, and non-contact method that has garnered considerable attention in ITO ablation.

During the laser ablation of ITO, if the photon energy of the irradiated beam is greater than the bandgap, electrons are excited from the valence band to the conduction band. The excited electrons absorb photon energy and transfer energy to the surrounding lattice, and ablation takes place as the electrons absorb energy [10, 11]. If the photon energy of the irradiated beam is less than the excitation energy, excitation does not take place, and electrons do not absorb energy. However, if the pulse of laser beam has short width, high intensity, and is focused to a small incident area, tunneling ionization can take place because of the distortion of the energy band due to light and electric fields; also, multiphoton absorption can be caused by the overlapping excitation. As a result, free electrons are generated in the irradiated area. Laser irradiation is often followed by heating of electrons, transfer of their energy to the surrounding lattices, and energy loss. As the energy is transferred to the surrounding area, avalanche ionization occurs ionizing the surrounding area [12–14].

Ultrafast lasers have been widely used in recent studies on ablation processes because the time taken for a single pulse to be irradiated is shorter than the time taken for the transfer of heat to the surroundings due to the short pulse width of the ultrafast laser. This also results in negligible

✉ Sung-Hak Cho
shcho@kimm.re.kr

Junha Choi
cjh426629@kimm.re.kr

¹ Department of Nano-Mechatronics, Korea University of Science and Technology, Daejeon, South Korea

² Department of Nano-Manufacturing Technology, Nano-Convergence Manufacturing Systems Research Division, Korea Institute of Machinery and Material, Daejeon, South Korea

thermal diffusion towards the periphery, improving spatial resolution [10, 15–17]. Therefore, ablation with an ultrafast laser is used in micromachining, OLED repair, fine 3D structure production, and Laser-assisted in situ keratomileusis (LASIK) and Laser-assisted sub-epithelial keratectomy (LASEK) [14, 18–24].

Various studies have been conducted to achieve high-resolution patterning on ITO by controlling the pulse duration, pulse energy, and the number of pulses [7, 8, 20, 25–29]. However, very few studies have analyzed ablation characteristics by simultaneously controlling the above conditions and wavelength. In this study, we investigated the influence of the ablation characteristics of pulse duration, pulse energy, number of pulses, and wavelength. We show that optimizing the ablation characteristics can lead to the highly efficient ablation of ITO.

2 Methods and Materials

2.1 System and Schematic Diagram

In this study, we used the Pharos SP model (Light Conversion) laser, with a fundamental wavelength of 1026 nm, tunable wavelengths of 513 nm and 355 nm, a minimum pulse duration of 164 fs, and a pulse duration of up to 10 ps. This laser has a maximum repetition rate of 200 kHz and maximum pulse energy of 1 mJ. Moreover, it supports the single-pulse operation. The experiment was conducted using pulse durations of 164 fs, 1 ps, and 10 ps with a repetition rate of 6 kHz, and we compared the characteristics at wavelengths of 513 nm and 1026 nm. The Fig. 1 shows the schematic optical setup of the femtosecond laser ablation system used in this study. The

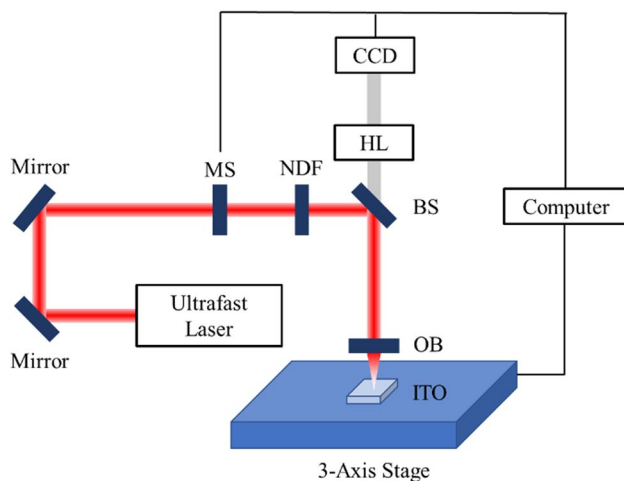


Fig. 1 Schematic of the ultrafast laser machining system (MS: Mechanical shutter, NDF: Neural density filter, BS: Beam splitter, OB: Objective lens, CCD: Camera, HL: Halogen lamp)

beam was transferred to the objective lens (OB; Mitutoyo, M Plan Apo NIR 20X, NA 0.40) through mirrors and beam splitter (BS). We employed a combination of a mechanical shutter (MS) and a neutral density filter (NDF) to control the transmission of the beam and regulate its energy density, respectively. After passing through OB, the laser beam was focused on the ITO sample for ablation. The ablated area was imaged using a confocal microscope (VK-X1000 Series) (KEYENCE). Moreover, 5 nm of Cr and 45 nm of Au were deposited using a Korea vacuum E-beam evaporator (KVET-C500200) to avoid electron charging during the scanning electron microscope (SEM) imaging and analyzed using a field emission-scanning electron microscope (FE-SEM) (S-4800) (Hitachi). An ITO thin film with a thickness of 250 nm was used as the ablation target sample.

2.2 Ablation Threshold

The ablation threshold is determined by using lasers under various conditions, including pulse energy and duration. The energy of the point at which the ablation begins is set as the ablation threshold. Alternatively, Liu et al. [30, 31] reported a method using Eqs. (1)–(3) with nonlinear fitting approach to determine the ablation threshold. In these equations, r is the radius of the ablated area, ρ is the radius of the incident beam, τ is the temporal radius, t is the time variable, E_0 is the fluence, and E_{th} is the ablation threshold. Equation (1) exhibits Gaussian spatial and temporal profile. The spatial distribution of the fluence is given by Eq. (2). In Eq. (2), r and E_0 can be expressed as in Eq. (3). Using these equations, ablation threshold can be calculated. Furthermore, there are other methods to determine ablation threshold. Kautek et al. [32] analyzed the visible damage caused by the formation of the ablation area, and the point irradiated by multiple pulses, where the ablated volume became null, was set as the ablation threshold. Lenzner et al. [33] irradiated 50 pulses, and the point at which the ablated volume became null was designated as the ablation threshold using the characteristic that the ablated volume varies linearly with the change in energy. The ablation threshold is affected by the wavelength, pulse duration, number of irradiated pulses, and surrounding environment, which include temperature and humidity. Therefore, even if the ablation threshold is obtained using a given material and method, different results can be obtained each time. In this study, the ablation threshold was determined when the ablation diameter became null for a single pulse.

$$I(r, t) = I_0 \exp(-r^2/\rho^2) \exp(-t^2/\tau^2) [30, 31] \quad (1)$$

$$E(r) = \int_{-\infty}^{\infty} dt I(r, t) = E_0 \exp(-r^2/\rho^2) [30, 31] \quad (2)$$

$$r^2 = \rho^2 (\ln E_0 - \ln E_{th}) [30, 31] \quad (3)$$

3 Results

3.1 ITO Ablation Threshold at 513 and 1026 nm

Based on Eqs. (1)–(3), we investigated the ablation threshold using a pulse duration was 164 fs with 513 and 1026 nm laser. To obtain the diameter of the ablated area required for calculating the ablation threshold, the pulse energy of a single pulse was adjusted before irradiating. Figure 2a shows the pulse energy of the irradiated pulse and the diameter of the ablated area, and Fig. 2b shows the ablation threshold obtained using nonlinear fitting. In this case, increasing the irradiated energy resulted in an increase in the ablated area. The ablation area increased until it became saturated. The ablation threshold was obtained using the ablation diameter and Eqs. (1)–(3). In Fig. 2b, the x-intercept (the point where the ablation diameter is 0) indicates the ablation threshold, which is calculated by extrapolating expression obtained using nonlinear fitting. In Fig. 2b, r represents the radius of the ablation area, and the fluence when r^2 becomes 0 indicates the ablation threshold. The ablation threshold acquired at 164 fs was found to be 0.68 J/cm² at 513 nm and 0.66 J/cm² at 1026 nm [8, 20, 34]. Figure 2b shows similar ablation threshold at 513 and 1026 nm wavelengths, respectively.

The similar ablation threshold at different wavelengths can be explained by the combination of linear and non-linear optics. According to Krause et al. [27], the absorption coefficient of ITO is approximately $4.1 \times 10^3 \text{ cm}^{-1}$ at 1026 nm and $2.1 \times 10^3 \text{ cm}^{-1}$ at 513 nm. This implies that in linear terms, 1026 nm has an absorption coefficient that is approximately twice as high as 513 nm. In nonlinear terms, ITO has fewer free electrons than metals because ITO is a semiconductor with wide bandgap. Thus, for energy to be absorbed by ITO, electrons should be excited first [35]. Excitation of electrons requires the photon energy of the laser to be higher than the bandgap. Carey et al. [36, 37] reported a 3.5 eV bandgap for the ITO, and Kim et al. [38] reported bandgap which is over to be 3.8 eV. In the case of the 1026 nm laser, it has a photon energy of 1.21 eV, and the 513 nm laser has a photon energy of 2.42 eV through Eq. (4). Owing to these values, a nonlinear phenomenon must occur to generate electrons for absorption, and in this study, excitation was generated using a femtosecond laser. Therefore, in nonlinear terms, the difference in the probability of occurrence of electrons is two times greater at 513 nm than that at 1026 nm. Due to the independence of linear optics and nonlinear optics, mutual cancellation occurs. As a result, it is assumed that similar ablation threshold values are calculated at wavelengths of 513 nm and 1026 nm.

$$E = \frac{hc}{\lambda} [38] \quad (4)$$

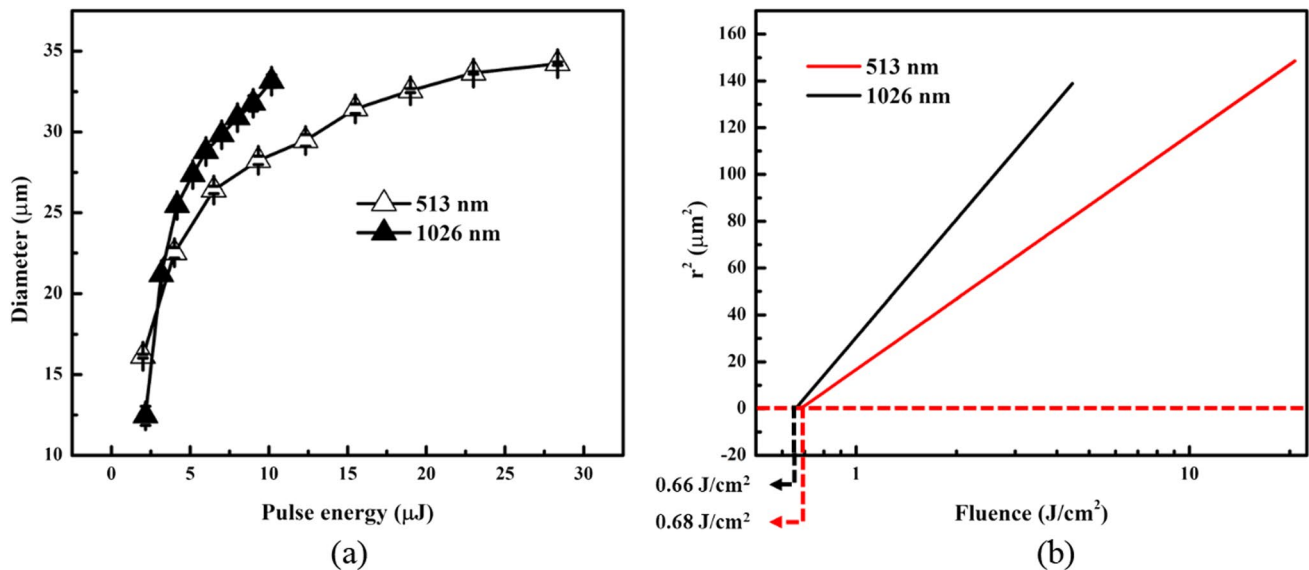


Fig. 2 a Diameter of the ablation area on ITO at 164 fs: for a higher fluence, the ablation area is larger. (each measurement is repeated ten times, triangle represent the average of ten data points). b Ablation threshold of ITO at 513 and 1026 nm

3.2 Effect of Fluence on Ablation Morphologies

In this study, the ablation characteristics at 513 nm and 1026 nm were compared under the same pulse energy conditions. The fluence should be considered before comparing the pulse energies. According to Eq. (5), the ablation diameters are different at different wavelengths. For different wavelengths, if the same pulse energy was applied, different values of pulse energy per unit area were irradiated. Commonly, Eq. (5) is referred to as the beam divergence [39]. In Eq. (5) [39], θ is the beam divergence, λ is the wavelength, and ω_0 is the waist radius. As a result, to achieve the same fluence (pulse energy per unit area), the pulse energy at 1026 nm should be set four times higher than that at 513 nm. Figure 3 shows an ITO image in which the same fluence is irradiated by setting pulse energy of 10 μJ at 513 nm and 40 μJ at 1026 nm. The ablation diameter of 1026 nm had a larger value for all pulse durations than that of 513 nm. This can be attributed to the larger beam diameter of 1026 nm compared to 513 nm, coupled with the higher absorption coefficient of ITO at 1026 nm, which is approximately two times higher than at 513 nm. At 164 fs and 1 ps, materials are ablated into a shape similar to that of a Gaussian beam, while at 10 ps, they are ablated into a flat shape. At

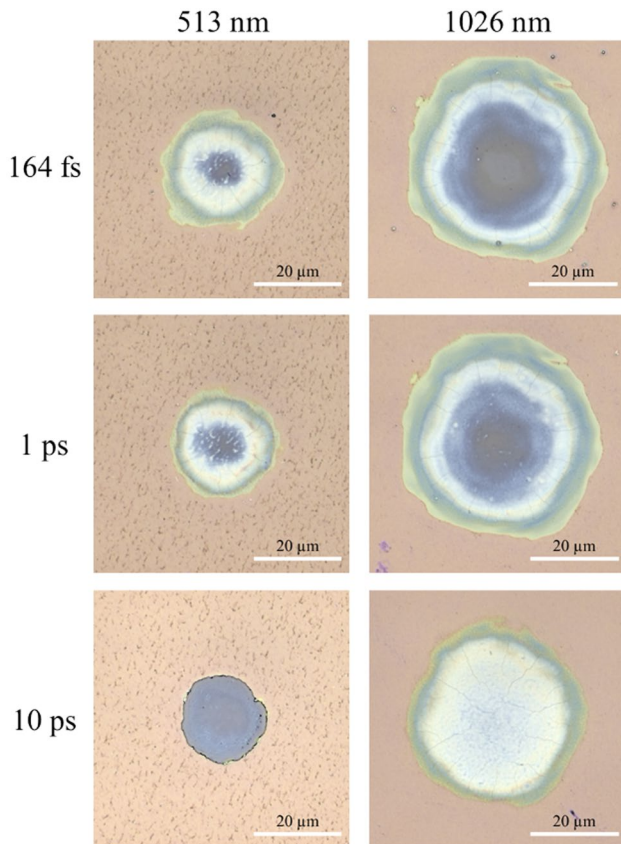


Fig. 3 Comparison of ITO ablation with equal fluences

1026 nm, a relatively larger amount of pulse energy is irradiated compared with that at 513 nm, and distinguishing the changes according to the pulse energy is difficult due to the relatively thin ITO thickness of 250 nm. Therefore, in subsequent experiments, the same pulse energy was fixed, and the ablation characteristics were compared.

$$2\theta = \frac{4\lambda}{\pi(2\omega_0)} [39] \quad (5)$$

3.3 Effect of Pulse Energy on Ablation Morphologies

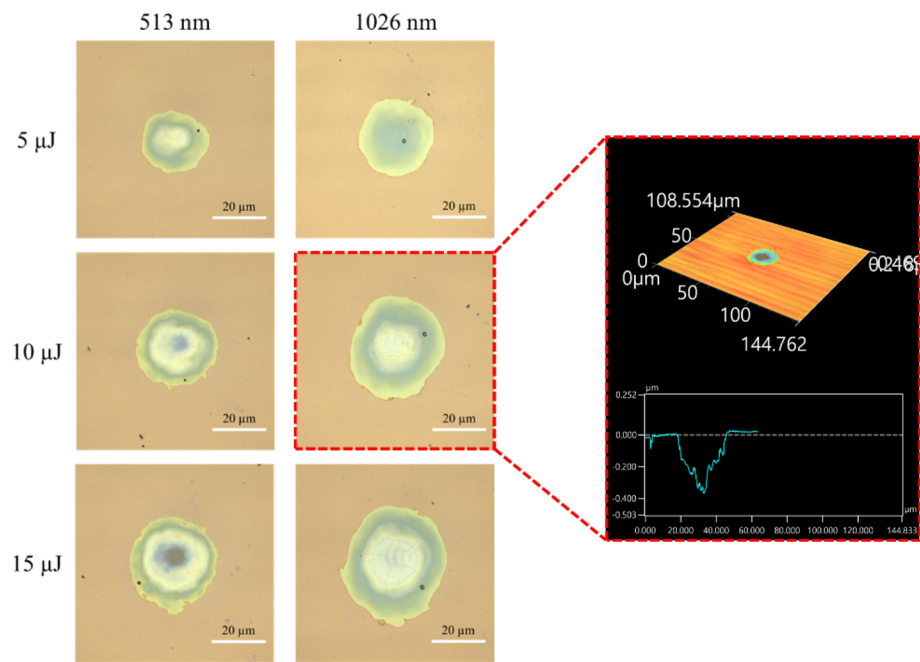
Ablation does not take place at extremely low pulse energies and only starts when the pulse energy exceeds the ablation threshold. However, if an excessively high energy pulse is irradiated, it may damage the glass substrate under ITO. To investigate the ablation characteristics in relation to pulse energy, pulse energies of 5, 10, and 15 μJ were focused on the ITO using a pulse duration of 164 fs and a single pulse. Figure 4 shows the ablation image and ablation diameter obtained by controlling the pulse energy. At 513 nm, the ablation diameter varied from 25 to 32 μm , and at 1026 nm, the ablation diameter varied from 27 to 37 μm . At both the wavelengths, the ablation diameter increased with increasing pulse energy. Despite the larger fluence at 513 nm, the ablation diameter at this wavelength was smaller than that at 1026 nm, due to the change in the beam size according to Eq. (4). Eventually, the ablation area reached saturation and ceased to increase further beyond a certain energy value. The ablated area exhibited a hemispherical shape due to the Gaussian beam and 164 fs pulse duration. Consequently, the central area was more ablated than the outer area, as observed in the confocal image and 2D morphology profile of Fig. 4a.

The outer edge area is visible through the FE-SEM image in Fig. 5. This edge part was ablated with a pulse duration of 164 fs, and a sharp edge was formed. An increase in the pulse energy had no significant effect on the edge part. This observation demonstrates the nonthermal properties of the femtosecond laser.

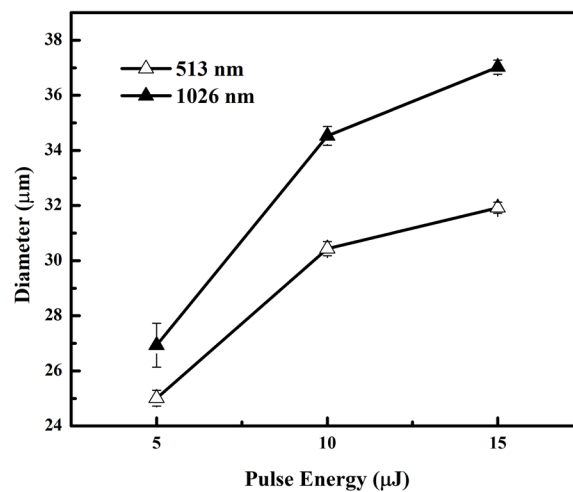
3.4 Effect of Pulse Duration on Ablation Morphologies

The most noticeable effect of changing the pulse duration is the change in heat generation. As the pulse duration increases, heat diffusion is activated, and the heat-affected zone grows in size. To investigate the change in ablation characteristics as a function of pulse duration, the ITO was irradiated using a single pulse with a pulse energy of 10 μJ , but with varying pulse durations of 164 fs, 1 ps, and 10 ps.

Fig. 4 a Confocal microscopy images of the ablation area. Here, the pulse energy is varied.
b Diameter of the ablation area on ITO as a function of the pulse energy at 164 fs and 513 and 1026 nm



(a)



(b)

Figure 6 shows the ablation image and ablation diameter obtained by controlling the pulse duration. At 513 nm, the ablation diameter varied from 20 to 27 μm, and at 1026 nm, the ablation diameter varied from 27 to 35 μm. Increasing the pulse duration at the same pulse energy results in decreased pulse intensity and ablation diameter. At 10 ps, for the same beam size, the maximum heat diffusion took place. However, the intensity was low, and thus, the ablation diameter was the smallest. Figure 6b shows that the ablation diameter at 513 nm is smaller than that at 1026 nm. Because the same pulse energy was irradiated at different wavelengths, the fluence was larger at 513 nm, but the beam size was larger at 1026 nm according to Eq. (4); therefore, 1026 nm laser rendered a larger ablation diameter. The

overall shape of the ablation area was hemispherical due to the Gaussian beam, with the central area exhibiting more ablation than the outer area. However, at 10 ps, the ablation surface appeared relatively flat compared to the other conditions. These characteristics were observed by confocal microscopy image and 2D morphology profile. At 10 ps, the relatively long pulse duration caused increased diffusion of heat, ionizing the surrounding area and ablating the ITO [17, 26].

For the edge part, there was a considerable difference with the change in the pulse duration. At 164 fs, the edge part was ablated sharply because it was only slightly affected by heat diffusion owing to the short pulse duration. The pulse duration of 1 ps also exhibited a sharp edge, which was

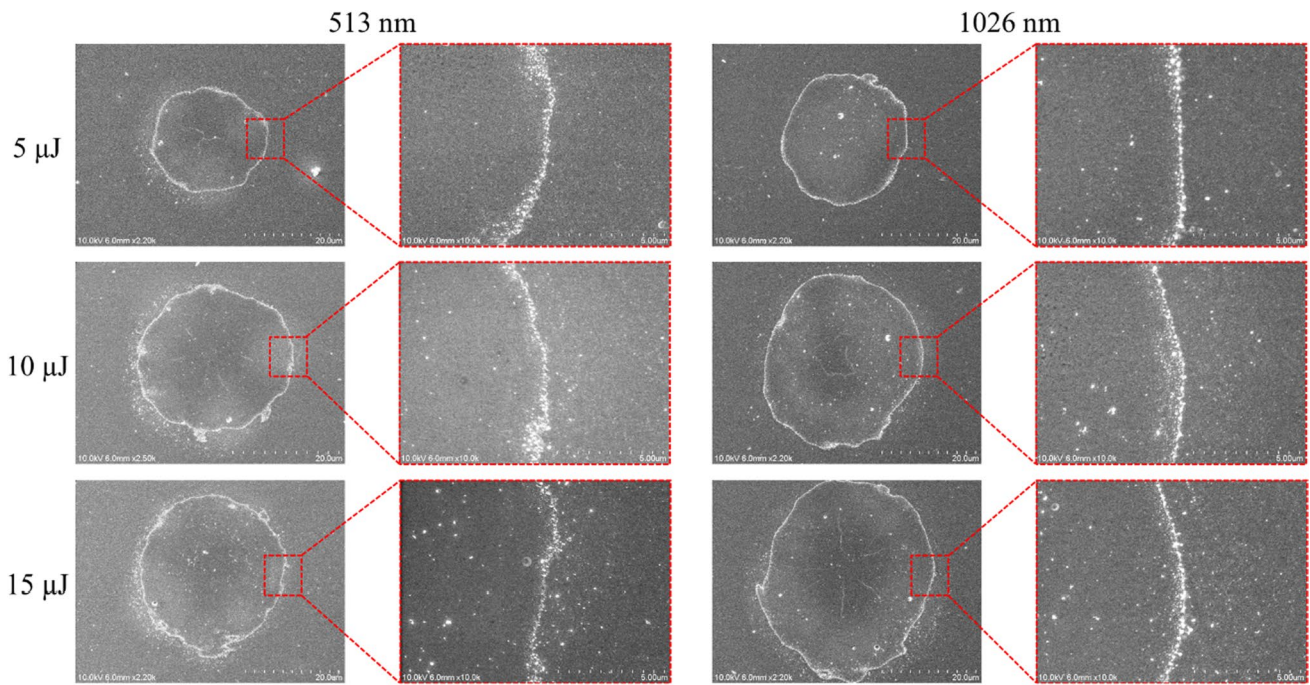


Fig. 5 SEM images of the area shown in Fig. 4 (the entire ablated portion and the edge portion)

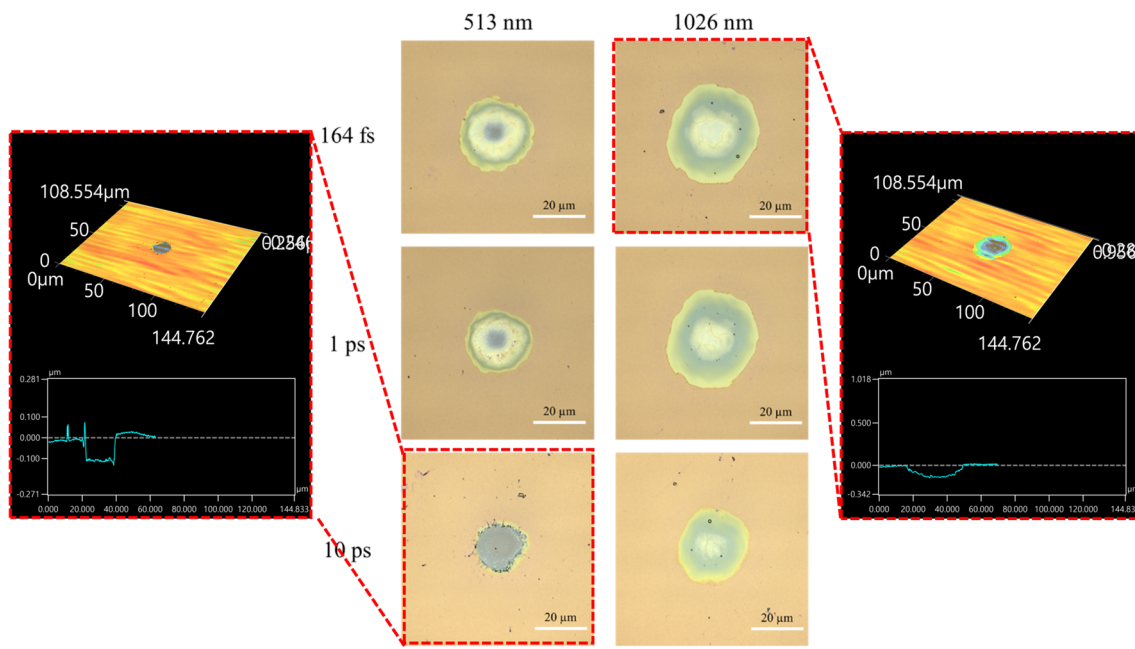
negligibly different from the pulse duration of 164 fs. For the 10 ps pulse, heat diffusion became non-negligible, and the non-thermal characteristics of the short pulse duration subsided [26]. As shown in Fig. 7, at 10 ps, the edge part, which was blunt compared to that for other pulse durations, can be observed. At 10 ps, the edge appeared blunt, and the morphology exhibited deformation due to heat. Thus, a wider pulse duration resulted in a blunt edge part. At 10 ps, the pulse intensity was low, resulting in relatively weak ablation compared to the narrower pulse duration. Because of the above characteristics, the sharpness of the edge is expected to improve as the pulse duration decreases. Further, 513 nm laser exhibited more pronounced changes. This is because, at the same pulse energy, the differences observed are attributed to the combination of the wider pulse duration of 10 ps and the higher fluence deposited on the ITO at 513 nm compared to 1026 nm.

3.5 Effect of the Number of Pulses on Ablation Morphologies

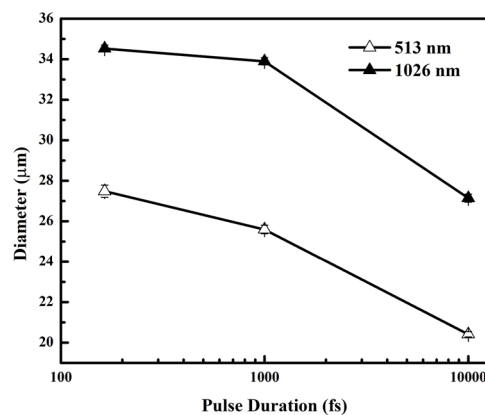
One way of obtaining the desired ablation size and edge is by changing the number of pulses. To investigate the effect of the number of pulses on the morphology, ITO was ablated using a pulse laser with a pulse energy of 10 μJ , a repetition rate of 6 kHz, and a pulse duration of 164 fs, while varying the number of pulses from one to five. As shown in Fig. 8, at 513 nm, the ablation diameter varied from 26 to 29 μm , and at 1026 nm, it varied from 36 to

38 μm . As explained in the previous section, the 1026 nm wavelength has a wider beam size and wider ablation diameter (Eq. 4). As the number of pulses increased, the ablation area also increased. This suggests that if the number of pulses increased before the saturation of ablation area, the ablation area became wider. However, as shown in Fig. 8, there is no significant difference in diameter with increasing pulse number because the pulse energy at $n = 1$ is sufficient for ablation. Therefore, additional pulses exhibit changes in the depth characteristics, rather than affecting the diameter. Femtosecond lasers have non-thermal properties owing to their short pulse duration, but heat is continuously accumulated on the surface of the ITO as pulses are irradiated. The accumulated heat melts the ITO and overlaps with the subsequent irradiated pulses, resulting in a larger ablation [40]. Moreover, by irradiating several pulses, additional damage to the glass substrate in the central region of the Gaussian beam was observed after the ITO was ablated at 513 nm. This is due to the higher fluence and photon energy of the 513 nm laser compared to the 1026 nm laser, despite having the same pulse energy.

As shown in the previous section, a sharp edge was observed at 164 fs. This sharp edge was observed when a single pulse was irradiated. However, when multiple pulses were irradiated at the same point, the accumulated heat led to an acceleration of heat diffusion and the formation of a wider heat-affected zone. Thus, if many pulses are irradiated, the thermal diffusion would increase, and unsharp edges will be observed. Figure 9 shows the FE-SEM image



(a)



(b)

Fig. 6 **a** Confocal microscopic images of the ablation area for different pulse durations. **b** Diameter of the ablation area on ITO as a function of the pulse duration at a pulse energy of $10 \mu\text{J}$ and wavelengths of 513 and 1026 nm

of the area shown in Fig. 8a. As can be seen in Fig. 9, when the first pulse was irradiated, a sharp edge was formed. Upon further irradiation of subsequent pulses, the morphology of the edge lost its initial sharpness. Additional ablation may occur at the edge due to the successive pulses, but the overall effect is similar to having a blunt edge due to the increased heat deposition.

3.6 Effect of Combined Laser Parameters on Ablation Morphologies

Figure 10 shows the results of an experiment where all the conditions adjusted in the previous sections were applied. The pulse duration was tuned to 164 fs, 1 ps, and 10 ps; the

pulse energy was set to 5, 10, and 15 μJ , and the number of pulses was adjusted from 1 to 5, increasing one pulse at a time. The ablation diameter observed in Fig. 10 are also depicted in Fig. 11. In summary, a larger ablation occurred when the pulse duration decreased, pulse energy increased, and the number of pulses increased. The largest diameter was obtained at a pulse duration of 164 fs, pulse energy of 15 μJ , 5 pulses, and 1026 nm wavelength. The smallest diameter was obtained at 10 ps, 5 μJ , 1 pulse, and 513 nm. Furthermore, the edge part appeared sharper as the pulse duration and number of pulses decreased, consistent with the previously observed characteristics. Regarding the edge part, no significant difference was observed between 164 fs and 1 ps, but distinct differences were evident at

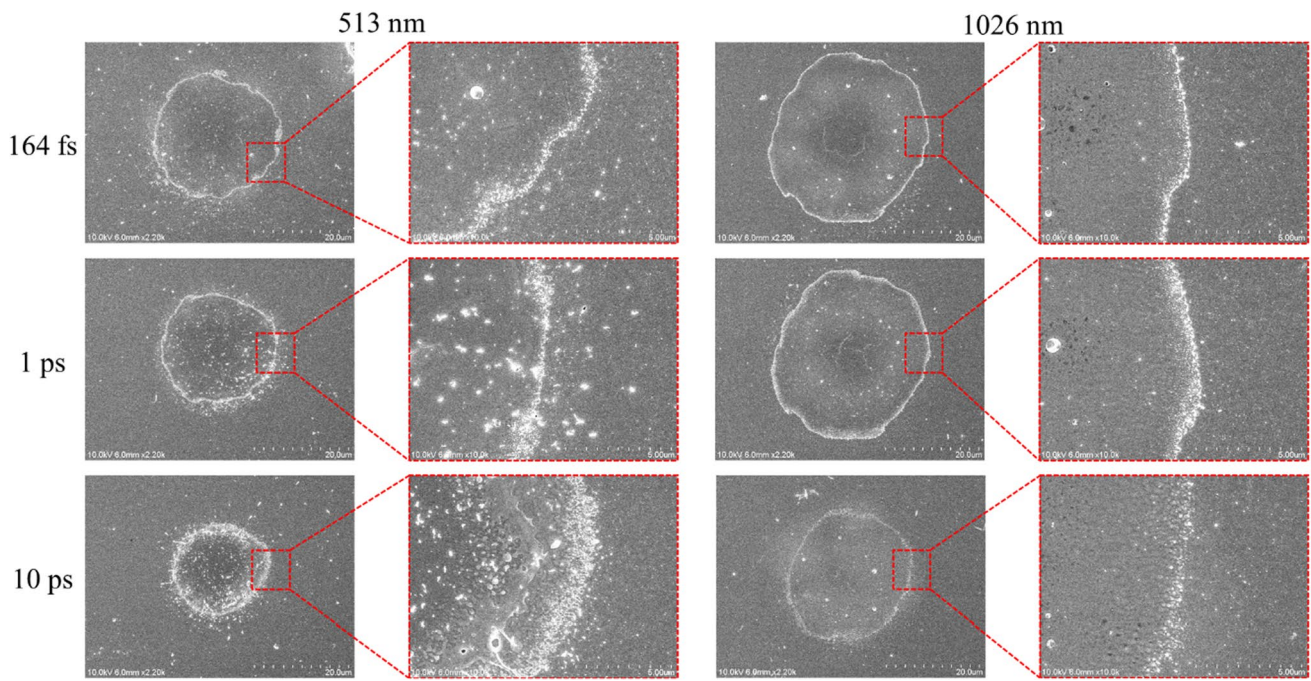


Fig. 7 SEM images of the area shown in Fig. 6 (the entire ablated portion and the edge portion)

10 ps. The sharpest edge was observed at a pulse duration of 164 fs and a single pulse, and a blunt edge was observed at 10 ps and many pulses. Overall, the ablation characteristics at 513 and 1026 nm exhibited similar trends for a given set of variables, but they differed in the terms of photon energy and spot size. To achieve the desired ablation shape with a sharp edge, a pulse duration of 164 fs, which ablates the same shape as the incident beam and creates a sharp edge area, was identified as the optimal parameter.

4 Conclusion

In this paper, an ultrafast laser was used to investigate the ablation characteristics under different conditions. The ablation threshold was obtained at each wavelength, and experiments were conducted based on the same pulse energy conditions. This study proposed a hypothesis to explain the similar ablation threshold for ITO at 513 nm and 1026 nm wavelengths, attributing it to the mutual cancelation of the effects of linear and nonlinear optics. We obtained a large ablation diameter for a large number of pulses having high

intensity and short duration. Depending on the conditions, the ablation characteristics and edge parts exhibited distinct modifications, following specific tendencies. Furthermore, in addition to the pulse energy standard, we introduced a method based on fluence to account for the energy per unit area. In this study, 513 and 1026 nm lasers were used, with the 513 nm laser having a smaller beam diameter than the 1026 nm laser at the same pulse energy. Consequently, to achieve matching fluence, four times the pulse energy must be applied at a wavelength of 1026 nm compared to that at 513 nm. According to Račiukaitis et al. [41], they compared ablation characteristic of ITO using UV and Green wavelengths. However, they employed a picosecond laser, which has different characteristic compared to a femtosecond laser. Therefore, we investigated ablation characteristic of ITO with 513, 1026 nm wavelengths first, and plan to investigate about ablation characteristic of ITO with UV femtosecond laser. In conclusion, this study contributed to determining the ablation tendencies under the same pulse energy and various other conditions. These findings have practical implications for utilizing ITO with variable ablation characteristics in relevant applications.

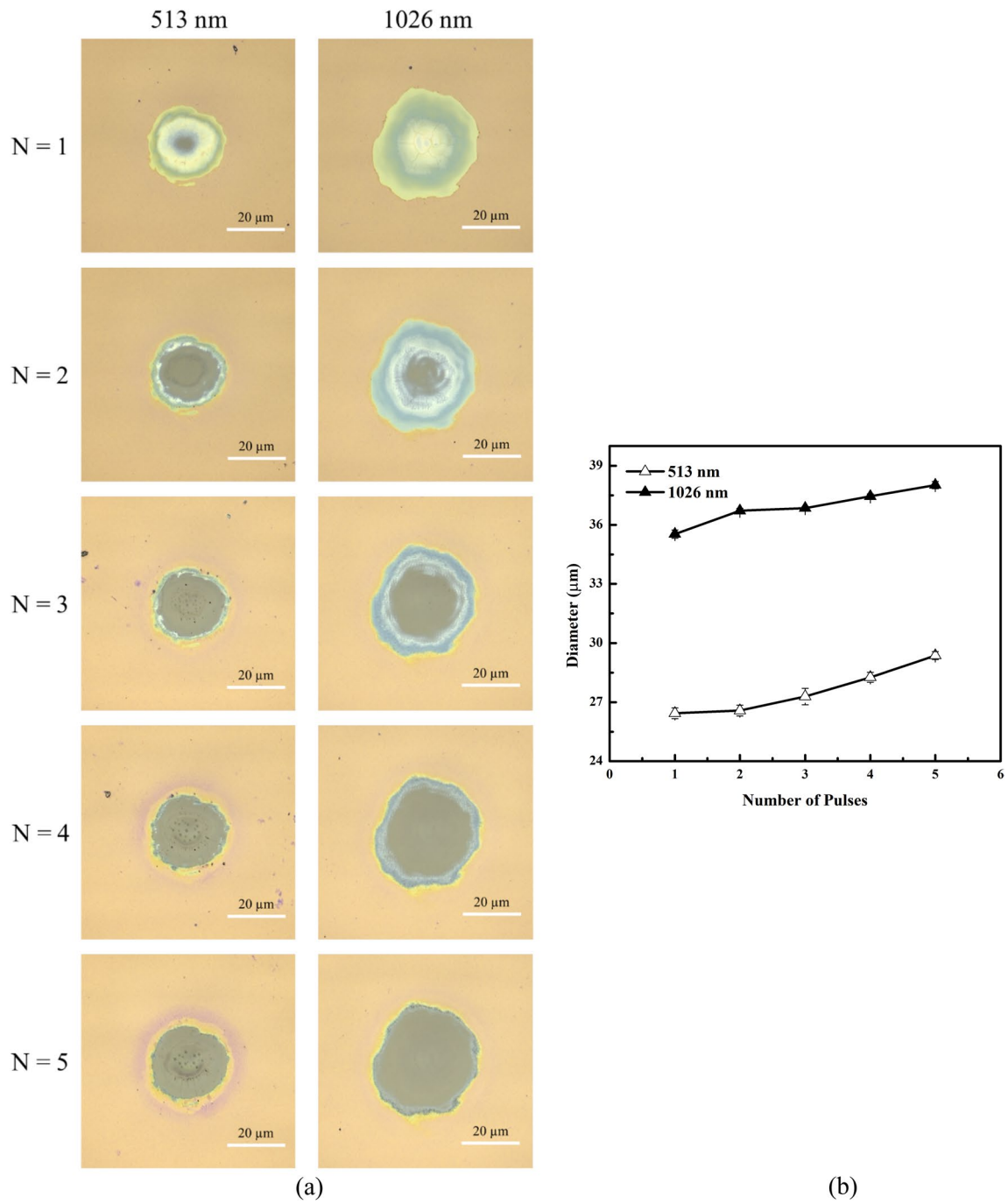


Fig. 8 **a** Confocal microscopic images of the ablation area for a different number of pulses. **b** Diameter of the ablation area on ITO as a function of the number of pulses at a pulse energy of 10 μJ, a pulse duration of 164 fs, and wavelengths of 513 and 1026 nm

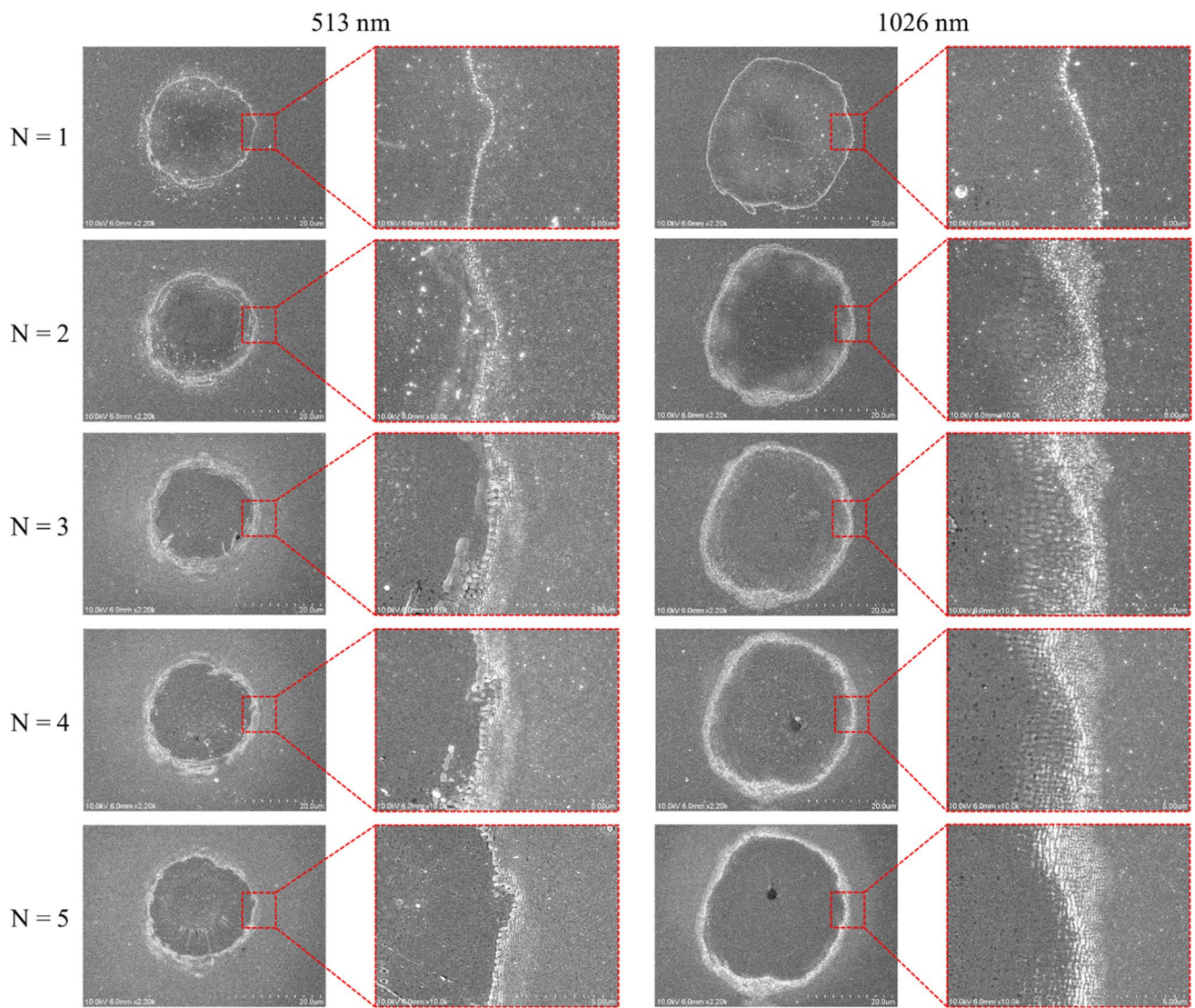


Fig. 9 SEM images of the area shown Fig. 8 (the entire ablated portion and the edge portion)

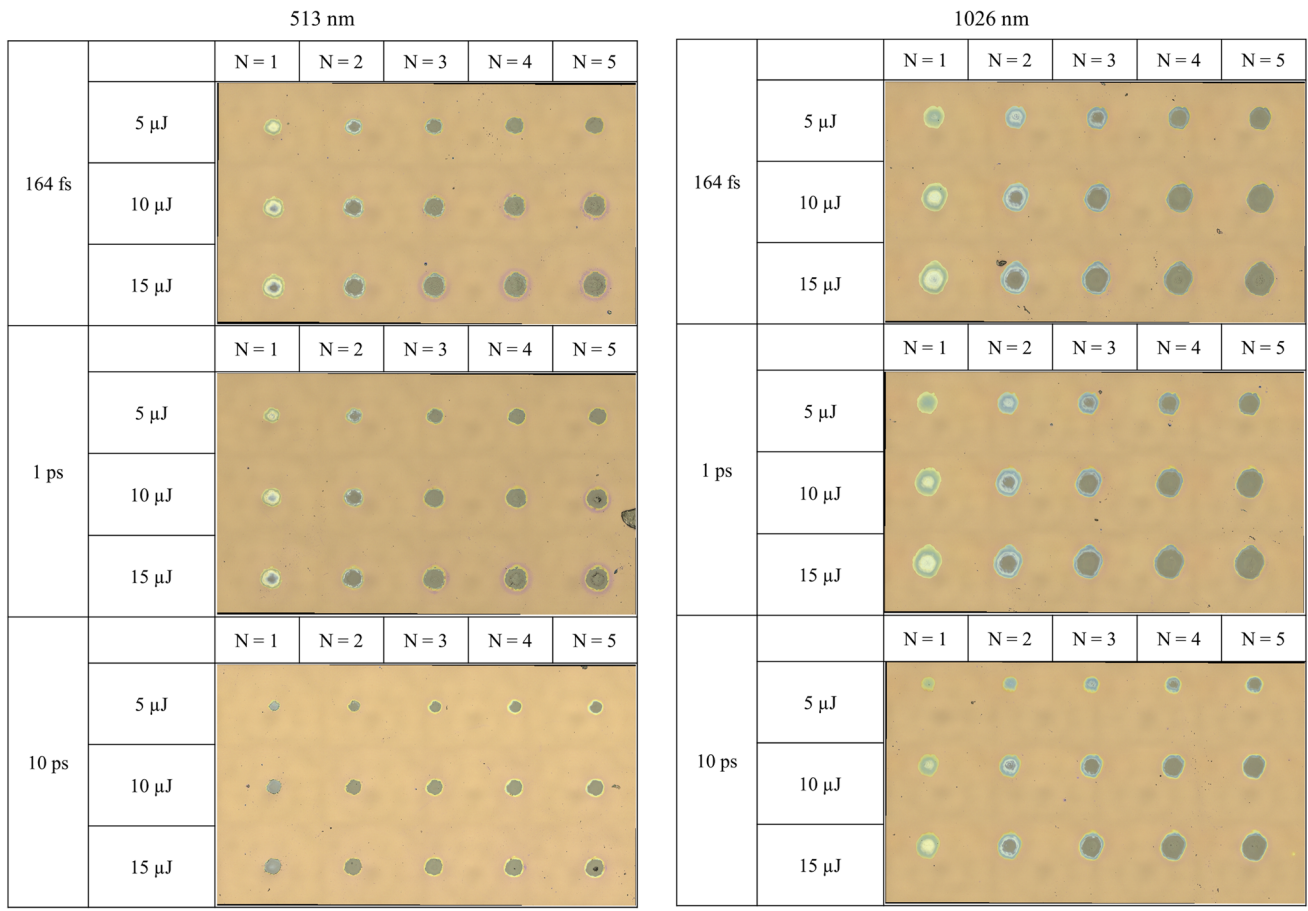


Fig. 10 Confocal microscopic images of the ablation area with the pulse energy, pulse duration, and the number of pulses as the variables

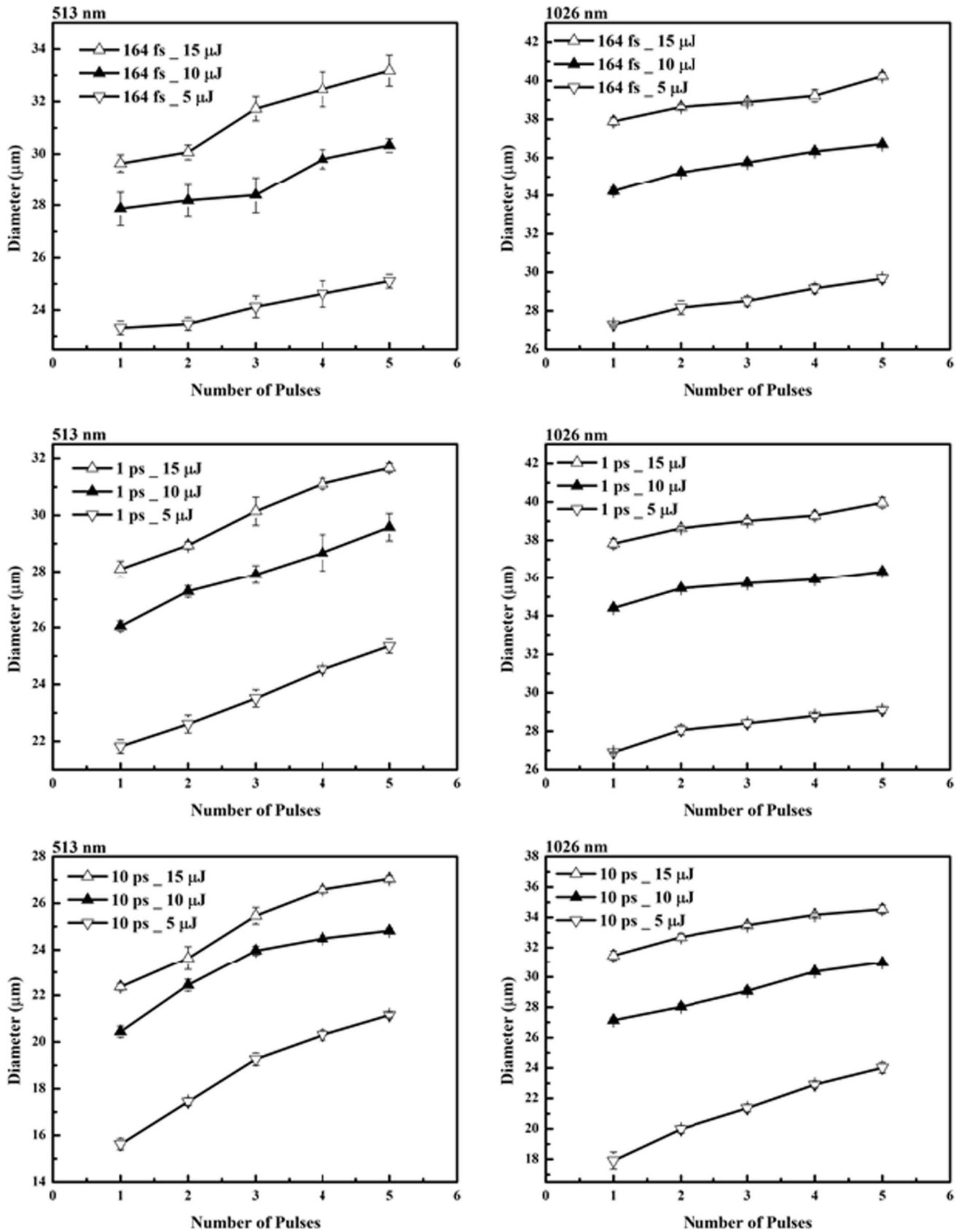


Fig. 11 Diameter of the ablation area on ITO as a function of pulse energy, pulse duration, and the number of pulses at 513 and 1026 nm

References

- Parthasarathy, G., Gu, G., & Forrest, S. R. (1999). Full-color transparent metal-free stacked organic light emitting device with simplified pixel biasing. *Advanced Materials*, *11*, 907–910.
- Hosokawa, C., Higashi, H., Nakamura, H., & Kusumoto, T. (1995). Highly efficient blue electroluminescence from a distyrylarylene emitting layer with a new dopant. *Applied Physics Letters*, *67*, 3853.
- Luff, B. J., Wilkinson, J. S., & Perrone, G. (1997). Indium tin oxide overlayers waveguides for sensor applications. *Applied Optics*, *36*, 7066.
- Chopra, K. L., Paulson, P. D., & Dutta, V. (2004). Thin-film solar cells: An overview. *Progress in Photovoltaics: Research and Applications*, *12*, 69–92.
- Rowell, M. W., & McGehee, M. D. (2011). Transparent electrode requirements for thin film solar cell modules. *Energy & Environmental Science*, *4*, 131–134.
- Liau, Y. H., Scherer, N. F., & Rhodes, K. (2001). Nanoscale electrical conductivity and surface spectroscopic studies of indium-tin oxide. *The Journal of Physical Chemistry B*, *105*, 3282–3288.
- Račiukaitis, G., Gečys, P., Trusovas, R., & Kondrotas, R. (2010). Picosecond laser scribing for thin-film solar cell manufacturing. In *Pacific International Conference on Applications of Lasers and Optics*. PICALO 2010.
- Bian, Q., Yu, X., Zhao, B., Chang, Z., & Lei, S. (2013). Femtosecond laser ablation of indium tin-oxide narrow grooves for thin film solar cells. *Optics & Laser Technology*, *45*, 395–401.
- Hoheisel, M., Mrotzek, C. (1991) *Microstructure and etching properties of sputtered ITO*, 461.
- Mirza, I., Bulgakova, N. M., Tomáščík, J., Michálek, V., Haderka, O., Fekete, L., & Mocek, T. (2016). Ultrashort pulse laser ablation of dielectrics: Thresholds, mechanisms, role of breakdown. *Science and Reports*, *6*, 1–11.
- Ben-Yakar, A., & Byer, R. L. (2004). Femtosecond laser ablation properties of borosilicate glass. *Journal of Applied Physics*, *96*, 5316–5323.
- Perry, M. D., Stuart, B. C., Banks, P. S., Feit, M. D., Yanovsky, V., & Rubenchik, A. M. (1999). Ultrashort-pulse laser machining of dielectric materials. *Journal of Applied Physics*, *85*, 6803–6810.
- Ams, M., Little, D. J., & Withford, M. J. (2012). *10-Femtosecond-laser-induced refractive index modifications for photonic device processing* (pp. P305-332). Woodhead Publishing.
- Sugioka, K., & Cheng, Y. (2014). Femtosecond laser three-dimensional micro- and nanofabrication. *Applied Physics Reviews*, *1*, 4.
- Nedialkov, N. N., Imamova, S. E., & Atanasov, P. A. (2004). Ablation of metals by ultrashort laser pulses. *Journal of Physics. D. Applied Physics*, *37*, 638–643.
- Ashkenasi, D., Müller, G., Rosenfeld, A., Stoian, R., Hertel, I. V., Bulgakova, N. M., & Campbell, E. E. B. (2003). Fundamentals and advantages of ultrafast micro-structuring of transparent materials. *Applied Physics A: Materials Science & Processing*, *77*, 223–228.
- Chichkov, B. N., Momma, C., Nolte, S., Von Alvensleben, F., & Tünnermann, A. (1996). Femtosecond, picosecond and nanosecond laser ablation of solids. *Applied Phys A*, *115*, 109–115.
- Sugioka, K., & Cheng, Y. (2012). Femtosecond laser processing for optofluidic fabrication. *Lab on a Chip*, *12*, 3576–3589.
- Pronko, P. P., Dutta, S. K., Squier, J., Rudd, J. V., Du, D., & Mourou, G. (1995). Machining of sub-micron holes using a femtosecond laser at 800 nm. *Optics Communication*, *114*, 106–110.
- Sugioka, K., & Cheng, Y. (2014). Ultrafast lasers-reliable tools for advanced materials processing. *Light Sci. Appl.*, *3*, 1–12.
- Yamamura, Y., Shimoyama, T., & Yan, J. (2022). Microscale surface patterning of zirconia by femtosecond pulsed laser irradiation. *International Journal of Precision Engineering and Manufacturing-Green Technology*, *9*, 619–632.
- Kim, B., Nam, H. K., Watanabe, S., Park, S., Kim, Y., Kim, Y. J., Fushinobu, K., & Kim, S. W. (2021). Selective laser ablation of metal thin films using ultrashort pulses. *International Journal of Precision Engineering and Manufacturing-Green Technology*, *8*, 771–782.
- Lee, H. M., Choi, J. H., & Moon, S. J. (2021). Machining characteristics of glass substrates containing chemical components in femtosecond laser helical drilling. *International Journal of Precision Engineering and Manufacturing-Green Technology*, *8*, 375–385.
- Shin, Y. G., Choi, J., & Cho, S. H. (2023). Morphologies of cemented tungsten carbides irradiated by femtosecond laser with high pulse energy for machining enhanced cutting tools. *International Journal of Precision Engineering and Manufacturing*, *24*, 547–553.
- Choi, H. W., Farson, D. F., Bovatsek, J., Arai, A., & Ashkenasi, D. (2007). Direct-write patterning of indium-tin-oxide film by high pulse repetition frequency femtosecond laser ablation. *Applied Optics*, *46*, 5792–5799.
- Stuart, B., Feit, M., Herman, S., Rubenchik, A., Shore, B., & Perry, M. (1996). Nanosecond-to-femtosecond laser-induced breakdown in dielectrics. *Physical Review B: Condensed Matter and Materials Physics*, *53*, 1749–1761.
- Krause, S., Miclea, P. T., Steudel, F., Schweizer, S., & Seifert, G. (2013). Precise microstructuring of indium-tin oxide thin films on glass by selective femtosecond laser ablation. *EPJ Photovoltaics*, *4*, 2–6.
- Park, M., Chon, B. H., Kim, H. S., Jeoung, S. C., Kim, D., Lee, J. I., Chu, H. Y., & Kim, H. R. (2006). Ultrafast laser ablation of indium tin oxide thin films for organic light-emitting diode application. *Optics and Lasers in Engineering*, *44*, 138–146.
- Ashkenasi, D., Lorenz, M., Stoian, R., & Rosenfeld, A. (1999). Surface damage threshold and structuring of dielectrics using femtosecond laser pulses: The role of incubation. *Applied Surface Science*, *150*, 101–106.
- Liu, J. M., Yen, R., Kurz, H., & Bloembergen, N. (1981). Phase transformation on and charged particle emission from a silicon crystal surface, induced by picosecond laser pulses. *Applied Physics Letters*, *39*, 755–757.
- Liu, J. M. (1982). Simple technique for measurements of pulsed Gaussian-beam spot sizes. *Optics Letters*, *7*, 196.
- Kautek, W., Krüger, J., Lenzner, M., Sartania, S., Spielmann, C., & Krausz, F. (1996). Laser ablation of dielectrics with pulse durations between 20 fs and 3 ps. *Applied Physics Letters*, *69*, 3146–3148.
- Lenzner, M., Krüger, J., Sartania, S., Cheng, Z., Spielmann, C., Mourou, G., & Kautek, F. (1998). Femtosecond optical breakdown in dielectrics. *Physical Review Letters*, *80*, 4076–4079.
- Baum, M., Strauß, J., Grübel, F., Alexeev, I., & Schmidt, M. (2014). Generation of phase-only holograms by laser ablation of nanoparticulate ITO layers. *Journal of Optics*, *16*, 12.
- Gamaly, E. G., Rode, A. V., Luther-Davies, B., & Tikhonchuk, V. T. (2002). Ablation of solids by femtosecond lasers: Ablation mechanism and ablation thresholds for metals and dielectrics. *Physics of Plasmas*, *9*, 949.
- Carey, P. H., Ren, F., Hays, D. C., Gila, B. P., Pearton, S. J., Jang, S., & Kuramata, A. (2017). Band offsets in ITO/Ga₂O₃ heterostructures. *Applied Surface Science*, *422*, 179–183.
- Kim, H., Gilmore, C. M., Piqué, A., Horwitz, J. S., Mattoussi, H., Murata, H., Kafafi, Z. H., & Chrisey, D. B. (1999). Electrical, optical, and structural properties of indium-tin-oxide thin films for organic light-emitting devices. *Journal of Applied Physics*, *86*, 6451–6461.

38. Pedrotti, F. L., Pedrotti, L. S., & Pedrotti, L. M. (2013). Introduction of optics (p. 6). Cambridge University Press.
39. Pedrotti, F. L., Pedrotti, L. S., & Pedrotti, L. M. (2013). Introduction to optics (p. 186). Cambridge University Press.
40. Di Niso, F., Gaudiuso, C., Sibillano, T., Mezzapesa, F. P., Ancona, A., & Lugarà, P. M. (2014). Role of heat accumulation on the incubation effect in multi-shot laser ablation of stainless steel at high repetition rates. *Optics Express*, 22, 12200.
41. Račiukaitis, G., Brikas, M., Gedvilas, M., & Rakickas, T. (2007). Patterning of indium-tin oxide on glass with picosecond lasers. *Applied Surface Science*, 253, 15.

Publisher's Note Springer Nature remains neutral with regard to jurisdictional claims in published maps and institutional affiliations.

Springer Nature or its licensor (e.g. a society or other partner) holds exclusive rights to this article under a publishing agreement with the author(s) or other rightsholder(s); author self-archiving of the accepted manuscript version of this article is solely governed by the terms of such publishing agreement and applicable law.



Sung-Hak Cho Principal Research Engineer in the Department Nano-manufacturing Technology, Korea Institute of Machinery and Material & Professor in the Department of Nano-Mechatronics, Korea University of Science and Technology. His research interest is Ultrafast-laser machining.



Junha Choi Ph.D. candidate in the Department of Nano-Mechatronics, Korea University of Science and Technology. His research interest is Ultrafast-laser machining.